Geophysical Research Letters

RESEARCH LETTER
10.1029/2018GL080601

Key Points:
- We calculated the value of polytropic index γ for Mercury's plasma sheet to be ~0.687, which is smaller than 5/3 (adiabatic)
- Nonadiabatic plasma behavior is driven by ion precipitation and ion demagnetization due to large loss cone and finite gyroradius effect
- We demonstrated that γ is lower during active time and determined a relationship between γ and the location of flow breaking region

Correspondence to:
G. Poh,
gangkai@umich.edu

Citation:
Poh, G., Slavin, J. A., Jia, X., Sun, W.-J., Raines, J. M., Imber, S. M., et al. (2018). Transport of mass and energy in Mercury's plasma sheet. *Geophysical Research Letters*, *45*, 12,163–12,170. https://doi.org/10.1029/2018GL080601

Received 26 SEP 2018
Accepted 12 NOV 2018
Accepted article online 15 NOV 2018
Published online 29 NOV 2018

Transport of Mass and Energy in Mercury's Plasma Sheet

Gangkai Poh[1], James A. Slavin[1], Xianzhe Jia[1], Wei-Jie Sun[1], Jim M. Raines[1], Suzanne M. Imber[2], Gina A. DiBraccio[3], and Daniel J. Gershman[4]

[1]Department of Climate and Space Sciences and Engineering, University of Michigan, Ann Arbor, MI, USA, [2]Department of Physics and Astronomy, University of Leicester, Leicester, UK, [3]Solar System Exploration Division, NASA Goddard Space Flight Center, Greenbelt, MD, USA, [4]Heliophysics Science Division, NASA Goddard Space Flight Center, Greenbelt, MD, USA

Abstract We examined the transport of mass and energy in Mercury's plasma sheet (PS) using MESSENGER magnetic field and plasma measurements obtained during 759 PS crossings. Regression analysis of proton density and plasma pressure shows a strong linear relationship. We calculated the polytropic index γ for Mercury's PS to be ~0.687, indicating that the plasma in the tail PS behaves nonadiabatically as it is transported sunward. Using the average magnetic field intensity of Mercury's tail lobe as a proxy for magnetotail activity level, we demonstrated that γ is lower during active time periods. A minimum in γ was observed at R ~ 1.4 R_M, which coincides with previously observed location of Mercury's substorm current wedge. We suggest that the nonadiabatic behavior of plasma as it is transported into Mercury's near-tail region is primarily driven by particle precipitation and particle scattering due to large loss cone and particle acceleration effect, respectively.

Plain Language Summary The transport process of mass and energy within Mercury's magnetotail remains unexplored until now. The availability of in situ magnetic field and plasma measurements from National Aeronautics and Space Administration's MErcury Surface, Space ENvironment, GEochemistry, and Ranging spacecraft provides us with the first opportunity to study the thermodynamic properties of particles within sunward convecting closed flux tubes in the plasma sheet. In this study, we study how mass and energy are transported in Mercury's magnetotail by investigating the relationship between the thermal pressure and number density of the plasma in Mercury's plasma sheet given by the equation of state in magnetohydrodynamics theory. We determined, for the first time, that the plasma behaves nonadiabatically as it is transported sunward toward Mercury. We suggest that precipitation of particles due to Mercury's large loss cone and demagnetization of particles due to finite gyroradius effect contributes to this nonadiabatic behavior of plasma in the plasma sheet. Our results have major implications in our understanding of particle sources and sinks mechanisms in Mercury's magnetotail.

1. Introduction

In situ magnetic field and plasma measurements observed by MErcury Surface, Space ENvironment, GEochemistry, and Ranging (MESSENGER) allowed us to understand the dynamics and structure of Mercury's magnetotail (Slavin et al., 2012) and plasma sheet (PS; DiBraccio, Slavin, Raines, et al., 2015; Poh et al., 2017a; Rong et al., 2018). Large-scale statistical studies have shown that processes occurring in Mercury's magnetotail are qualitatively similar to Earth's, despite the differences in spatial and temporal scales, upstream conditions, and internal plasma compositions (Gershman et al., 2014; Poh et al., 2017b; Raines et al., 2011). Mass, energy, and magnetic flux are transported from Mercury's dayside magnetopause to its nightside magnetotail via an Earth-like Dungey cycle (Imber & Slavin, 2017; Slavin et al., 2010). The cycle is completed by the return flow of mass, energy, and flux toward Mercury driven by magnetic reconnection in Mercury's PS (DiBraccio, Slavin, Imber, et al., 2015; Slavin et al., 2009; Smith et al., 2017; Sun et al., 2015; Sundberg et al., 2012; Zhong et al., 2018).

In order to understand mass, momentum, and energy transport through a planetary magnetotail, it is essential to understand the sunward convection of closed flux tubes and thermodynamic properties of particles within the PS (Baumjohann & Paschmann, 1989; Siscoe, 1983). In magnetohydrodynamics (MHD) theory, the local plasma pressure (P_i) can be expressed as follows:

$$P_i = \alpha n_i^{\gamma} \quad (1)$$

where n_i is the proton number density. The α is a constant related to the specific entropy of a particular flux tube. The polytropic index γ in equation (1) determines the type of thermodynamic process a closed flux tube experience as it is transported sunward. In an ideal, adiabatic system where there is no particle source or loss (i.e., reversible process) and no heat transfer in and out of the PS, it should be the case that $\gamma = 5/3$ or (~1.67). Indeed, this is the value of γ is commonly used in MHD simulations (e.g., Jia et al., 2015). If γ is less than 5/3, it means that the plasma behaves nonadiabatically (i.e., particle gain/loss or heat transfer or both). Equation (1) can be linearized as follows:

$$\log P_i = \gamma \log n_i + \log \alpha \tag{2}$$

γ may then be calculated by performing linear regression analysis on log (P_i) and log (n_i).

Baumjohann and Paschmann (1989) first determined the overall value of polytropic index for the Earth's PS using Active Magnetospheric Particle Tracer Explorer/Ion Release Module (IRM) plasma data under a wide range of conditions and regions and found it to be ~1.69, which is close to 5/3, suggesting adiabatic plasma behavior. On the other hand, using ISEE data, Huang et al. (1989) calculated a γ value of ~0.6, which would require that the plasma on a flux tube undergoing rapid contraction as it moves planetward to cool as opposed to heat due to compression. However, this value of 0.6 is closer to that determined by Schindler and Birn (1982) who produced a realistic variation of pressure with radial distance by inputting a value of $\gamma = 2/3$ in the equation of state. This avoided the unrealistic order-of-magnitude pressure increase in near-Earth magnetotail that arises when using $\gamma = 5/3$ from ideal MHD theory (Erickson & Wolf, 1980). Spence et al. (1989) determined a similar result using statistical averages of plasma pressure observed in the near-Earth magnetotail region. The 2/3 value was also used by Kivelson and Spence (1988) in their modified magnetotail model while investigating the effects of finite tail width. Borovsky et al. (1998) subsequently calculated γ to be ~1.52 using International Sun-Earth Explorer-2 data, while Pang et al. (2015) found a range of γ values from ~0.1 to 1.8 using Cluster data. More recently, Frühauff et al. (2017) obtained a γ of ~1.72 using Time History of Events and Macroscale Interactions during Substorms (THEMIS) data. Taken together, these results suggest that γ for Earth's PS is highly dependent on the data set used in the analysis.

MESSENGER's measurements of ion temperature and density (Andrews et al., 2007) and magnetic fields (Anderson et al., 2007) during its 4-year orbital mission around Mercury provide the first opportunity to investigate the transport of mass and energy in Mercury's PS. Here we will describe the method used to identify these intervals of MESSENGER's encounter with Mercury's PS. Using regression and statistical analysis of the plasma measurements, we calculated an average γ of ~0.687 and demonstrated a relationship between γ and substorm-related phenomenon in Mercury's PS.

2. MESSENGER Data Set and Event Selection

In this study, we analyzed the full-resolution one energy scan per 10-s plasma (Andrews et al., 2007) and 20 vectors per second magnetic field (Anderson et al., 2007) measurements from MESSENGER's Fast Imaging Plasma Spectrometer (FIPS) and Magnetometer, respectively. The accuracy of our calculated polytropic index is limited by our ability to observe the plasma in a given magnetic flux tube as it travels sunward. The assumption of constant specific entropy in each flux tube becomes a significant source of uncertainty since we do not know the flux tubes' history (Zhu, 1990). As a result, noise and biases may be introduced, which could influence our determination of γ at Mercury. Therefore, it is important to use the plasma measurements in its highest data resolution. However, due to its placement on the MESSENGER spacecraft, FIPS had limited field of view of the full proton distribution (See Gershman et al., 2013, for more details). This poses a challenge to accurately calculate the moments of the bulk PS population (i.e., plasma density and temperature) at Mercury in FIPS native resolution of 10 s per full scan of all energy levels. Therefore, we chose to use the 1-min averaged plasma moments derived from FIPS data.

We chose the Mercury Solar Magnetospheric (MSM) coordinate system for analyses performed in this study. The MSM coordinate system is centered on Mercury's internal offset dipole (Anderson et al., 2011). The *X* axis is positive in the sunward direction along the Sun-Mercury line, *Z* axis is positive northward parallel to Mercury's magnetic dipole moment axis, and *Y* axis completes the right-handed system. To account for solar wind aberration, we rotate the MSM *X* and *Y* axes by the solar wind aberration angle, which was calculated on

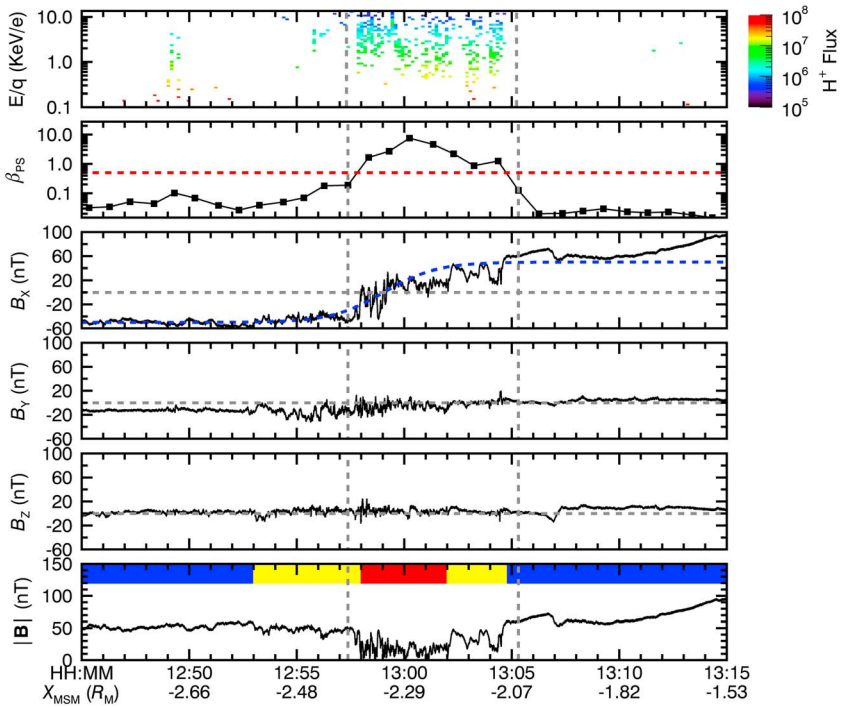

Figure 1. FIPS energy-per-charge spectrogram (first panel), plasma β (second panel), and magnetic field (third to sixth panels) measurements of MESSENGER crossing of Mercury's plasma sheet (PS) on 18 February 2012. The third panel shows the fitted Harris current sheet. Red, blue, and yellow color bars represent the PS, PSBL, and tail lobe (northern/southern) regions, respectively. Vertical lines represent the PS interval identified using the criteria $\beta \geq 0.5$.

a daily basis assuming a radial solar wind speed of 400 km/s, into the new aberrated MSM (or MSM') coordinate system.

Figure 1 shows an example of MESSENGER's traversal of Mercury's PS on 18 February 2012. First panel of Figure 1 shows the energy-per-charge (E/Q) spectrogram observed by FIPS. Second panel of Figure 1 shows the plasma β (i.e., thermal to magnetic pressure ratio) calculated using FIPS' plasma moments; *x*, *y*, and *z* components and magnitude (|**B**|) of the magnetic field measurements are shown in third to sixth panels of Figure 1, respectively. The interval starts with MESSENGER in the southern tail lobe, which is characterized by the low plasma β (~0.05), strong |**B**| (~50 nT) and low levels of fluctuation predominantly in the negative $B_{X'}$ direction. At ~UT 12:53, MESSENGER entered the southern plasma sheet boundary layer (PSBL), which is identified by moderate |**B**| fluctuations of ~10 nT (e.g., Slavin et al., 1985). MESSENGER then entered the PS at ~UT 12:58 shown by the further decrease of |**B**| to ~15 nT, reversal of $B_{X'}$ across the cross-tail current sheet, presence of 0.5- to 1-keV protons, and increase of β to ~10. Lastly, MESSENGER exited the PS into the northern PSBL, and subsequently into the high latitude, northern part of Mercury's dipolar, low β (~0.02) inner magnetotail region characterized by positive $B_{X'}$ and strong |**B**| of ~100 nT.

We visually identified a total of 759 PS crossings over four years of MESSENGER data using the following selection criteria:

1. Plasma β inside the PS and PSBL must be *greater than 0.5*.
2. A crossing of the cross-tail current sheet, identified by a clear reversal in $B_{X'}$ coincident with a depression in |**B**|, must be present.

Plasma β has been used extensively in many magnetotail studies to identify the boundary between the PS region (including the PSBL) and tail lobe. Terrestrial studies (e.g., Angelopoulos et al., 1994) used a range of β cutoff values from 0.1 to 0.5 to identify the boundaries of Earth's PS. In this study, we adopted the criteria used by Sun et al. (2016) to define Mercury's PS as the region with $\beta \geq 0.5$. The vertical lines in Figure 1 denote the PS boundary set by these criteria.

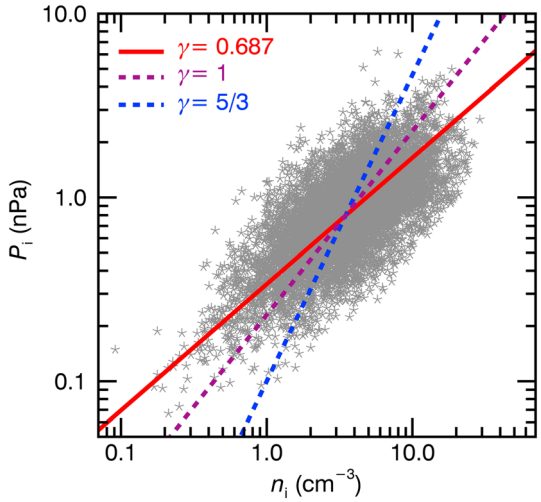

Figure 2. Logarithmic values of P_i versus n_i measured in 759 Mercury's plasma sheet crossings. The red line represents the orthogonal regression line. The purple and blue lines represents the P_i versus n_i relationship for $\gamma = 1$ (isothermal) and 5/3 (adiabatic).

3. Analysis

3.1. Polytropic Index

Figure 2 shows all P_i versus n_i measurements observed during the 759 PS crossings identified in this study. Note that both P_i and n_i axes have logarithmic scales. As shown in Figure 2, MESSENGER measured a large range of P_i and n_i during the PS encounters, ranging from 0.06 to 7 nPa and 0.08 to 30 cm^{-3}, respectively. Note that the high pressure and density measurements correspond to measurements made in the PS, while the low pressure and density measurements correspond to those measured in the PSBL. Figure 2 also clearly shows a linear relationship between the logarithmic values of P_i and n_i as indicated by the linearized equation of state (equation (2)). Correlation analysis yields a correlation coefficient (r) of ~0.684, which indicates that there is a linear relationship between log (P_i) and log (n_i), consistent with a single, well-constrained polytropic exponent.

Since this is a two-dimensional data set, we performed the Deming regression analysis (Deming, 1943) on the P_i versus n_i measurements, which accounts for errors in both variables (P_i and n_i) to compute the line of best fit. We also used the jackknife method (Linnet, 1990) to estimate the errors in the slope and y intercept of the regression line. The regression analysis yields a regression coefficient (i.e., polytropic index γ) of ~0.687 ± 0.008. Since the calculated value of γ is much smaller than 5/3 (~1.67), our result suggests that the plasma inside a contracting flux tube in the PS cools as it is transported sunward toward Mercury. This result also indicates that the plasma pressure in Mercury's inner magnetotail is lower than that predicted from the equation of state with γ = 5/3. There appears to be a net energy and particles lost from the flux tube during the convection process in Mercury's inner magnetotail. Implications of these results will be further discussed in section 4.

3.2. Dependence of Magnetotail Activity Level

We further examined the dependence of γ on the level of magnetotail activities. Earlier terrestrial studies on the determination of γ for Earth's PS (Frühauff et al., 2017, and references therein) show the importance of separating the P_i and n_i data set according to the activity level (i.e., quiet and active times) of the terrestrial magnetotail. A similar index based on the level of magnetic fluctuations observed within Mercury's magnetosphere was developed by Anderson et al. (2013). Here we used the average magnetic field intensity of Mercury's tail lobe ($|\mathbf{B}_{lobe}|$) instead for each identified PS crossing event as a proxy for activity level in Mercury's magnetotail. We assumed that $|\mathbf{B}_{lobe}|$ does not have spatial or temporal dependence during each PS crossing. The use of $|\mathbf{B}_{lobe}|$ as a first order approximation for Mercury's magnetotail activity is suitable because $|\mathbf{B}_{lobe}|$ tends to be higher during the growth and expansion phase (or active periods) of the substorm process and lower during quiet periods (e.g., Imber & Slavin, 2017, Sun et al., 2015).

Figure 3a shows the P_i and n_i diagram similar to Figure 2; the colors associated with each P_i and n_i measurements represent $|\mathbf{B}_{lobe}|$ for the corresponding PS crossing. It is clear that there are two different

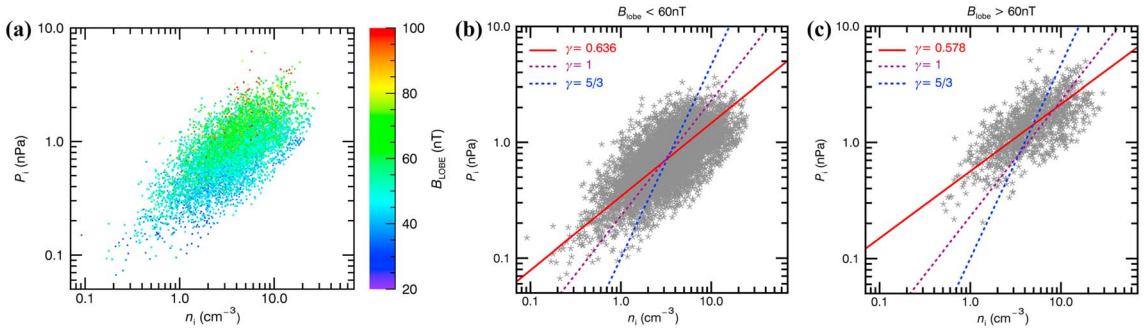

Figure 3. (a) Logarithmic values of P_i versus n_i measurements. Colors represents average magnetic field intensity of Mercury's tail lobe for each plasma sheet encounter. P_i versus n_i measurements during (b) active and (c) quiet times.

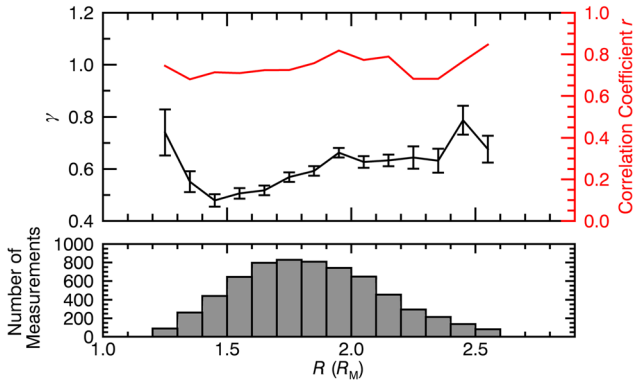

Figure 4. (top) Polytropic index γ and corresponding r versus radial distance R. P_i versus n_i measurements are sorted into bins of 0.1 R_M from R = 1.2 to 2.6 R_M. (bottom) Histogram of number of measurements in each bins.

groups of measurements distinguished by $|\mathbf{B}_{lobe}|$. It is expected that higher magnetic field intensity in the tail lobe leads to higher plasma pressure in Mercury's PS. Using a range of $|\mathbf{B}_{lobe}|$ threshold values, we determined that a threshold value of 60 nT best defines the two subsets of measurements representing quiet and active conditions. We separated the entire data set into two subsets for quiet (i.e., $|\mathbf{B}_{lobe}| < 60$ nT) and active (i.e., $|\mathbf{B}_{lobe}| > 60$ nT) magnetotails as shown in Figures 3b and 3c, respectively. The regression analyses yield a γ value of ~0.636 ± 0.008 and 0.58 ± 0.02 for the quiet and active data subsets, respectively. The correlation coefficient is ~0.68 for both subsets, indicating successful regression analyses. Our results show that γ is ~13% smaller during active than quiet times, which suggests that planetward convection is less adiabatic and more particles and energy are lost from the flux tube when Mercury's magnetotail is more active (i.e., during substorms).

3.3. Downtail Variation of γ in Mercury's PS

We examined the radial distance from Mercury (R) dependencies of the polytropic index γ. Using only measurements within ±1 R_M centered on the noon-midnight meridian, we binned the plasma measurements into radial bins of 0.1 R_M from R = 1.2 to 2.6 R_M and compute γ for each bin using the regression technique discussed in section 3.1. The calculated γ as a function of R is shown in the top panel of Figure 4. The error bars represent the standard errors of the calculated regression line parameters.

Our results show that the value of γ remains constant at ~0.65 between R = 2 R_M and R = 2.4 R_M. However, γ decreases steadily with decreasing radial distance from Mercury between 1.5 R_M and 2 R_M until it reaches a minimum at R ~ 1.4 R_M with γ ~ 0.45 before increasing to ~0.75 at R ~ 1.2 R_M. The relative size of the error bars and constant r for the measurements in all R bins (red line) at ~0.7 indicates that the minima in γ are unlikely to be the results of observational bias. The location of the minima in γ coincides with the location of Mercury's substorm current wedge identified by Poh et al. (2017b). A similar minimum in γ as a function of R was also observed in the terrestrial study by Frühauff et al. (2017). They suggested a connection between the decrease of γ and the flow-braking region typically observed at $X \sim -15$ R_M (e.g., Shiokawa et al., 1997). Our result also suggests a similar connection between the observed decrease in γ and the location of the flow-braking region in Mercury's inner magnetotail.

4. Summary and Discussion

MESSENGER observations of 759 crossings of Mercury's PS were examined and our results can be summarized as follows:

1. We calculated the average value of γ for Mercury's PS to be ~0.687.
2. We demonstrated that γ is lower during active times than quiet times.
3. The observed minimum in γ at R ~ 1.4 R_M indicates a relationship between decreases in γ and location of the flow braking region in Mercury's inner magnetotail.

The polytropic index γ determines the thermodynamic process a closed flux tube experiences as it is transported sunward. Our regression analysis of FIPS plasma measurements yielded a polytropic index γ of ~0.687 (or ~2/3) for Mercury's PS, which is smaller than the adiabatic polytropic index of 5/3. This result suggests that the plasma within the contracting, planetward moving flux tube *cools*, indicating net particle and energy loss, as the flux tube is transported into Mercury's low-β inner magnetotail region. Our calculated γ value is consistent with the γ = 2/3 value determined by some terrestrial studies based on their Earth's magnetospheric model (Kivelson & Spence, 1988; Schindler & Birn, 1982) and observations (Huang et al., 1989; Spence et al., 1989). Kivelson and Spence (1988) concluded that the effects of finite tail width and loss of particles through precipitation could account for the observed lower plasma pressure (i.e., γ = 2/3; Spence et al., 1989) in the near-tail region under the condition of steady state convection occurring in the magnetotail. The agreement between both our observations and simulation results from the Kivelson and Spence (1988) magnetospheric model strongly suggests that similar mechanisms might be occurring in

Mercury's PS that would result in our observation of $\gamma \sim 0.687$, which is not surprising considering the strength of Mercury's global magnetic field and the typical ion gyroradius (~380 km; DiBraccio, Slavin, Imber, et al., 2015) relative to the system size.

The two primary sink mechanisms for particles in Mercury's PS are (1) particle precipitation due to large loss cone and (2) nonadiabatic particle scattering due to strong acceleration processes. Earlier studies have shown that the loss cone for Mercury's magnetospheric cusp is uniquely large (e.g., Goldstein et al., 1981; Raines et al., 2014). The equatorial loss cone for Mercury's nightside magnetosphere ranges from ~13° to 23°, as compared to Earth's loss cone of $<3°$ beyond geosynchronous orbit (~6 R_E; Baumjohann & Treumann, 1996). As a result of Mercury's large loss cone, particles with sufficiently small pitch angles are likely to precipitate onto Mercury's high-latitude nightside surface and become lost from the flux tubes, instead of mirroring at the high-latitude mirror point and undergoing several bounce motions to become *trapped* within the flux tube, as in the case of Earth. This effect is further enhanced by Mercury's offset dipole magnetic field with more PS particle loss in the southern hemisphere surface (Korth et al., 2014). Furthermore, at Earth, outflow from the terrestrial ionosphere serves as a significant source of magnetospheric plasma for the terrestrial PS (Chappell et al., 1987), continually replenishing flux tubes as they propagate earthward. In contrast, Mercury's lack of an ionosphere means there is only a low flux of plasma, produced by photoionization and subsequent acceleration of exospheric ions, drifting into Mercury's magnetotail. This source is insufficient to refill flux tubes depleted by constant precipitation as they propagate into Mercury's inner magnetotail. Through this mechanism, Mercury's large loss cone contributes to the nonadiabatic behavior of plasma within a closed flux tube observed in this study.

Another reason for nonadiabatic plasma behavior at Mercury is scattering of particles due to the complex set of acceleration processes occurring in Mercury's magnetotail (e.g., Zelenyi et al., 2007). Solar wind and planetary ions in Mercury's PS are known to have large gyroradius relative to the scale length of magnetic field variations due to Mercury's weak intrinsic magnetic field. The influence of centrifugal force on particle motion becomes important in Mercury's PS due to finite gyroradius effects (Delcourt et al., 1996), thereby accelerating particles and resulting in nonadiabatic Speiser-type orbits (Delcourt et al., 2003) across magnetospheric regions. At Mercury, particles were also observed to be energized and accelerated near the X-line by magnetic reconnection (Zhong et al., 2018) and reconnection-related phenomena, such as dipolarization fronts (Dewey et al., 2017; Sun et al., 2017). Particle acceleration could result in the chaotic and nonadiabatic motion of particles (Büchner & Zelenyi, 1989), thereby resulting in the loss of particles within the flux tube during compressional convection and subsequent transport into another magnetospheric region, impact onto Mercury's nightside surface, or shadowing of the magnetopause. Therefore, the scattering of particles due to particle acceleration processes provides another plausible explanation of why $\gamma \sim 2/3$ (instead of 5/3) in Mercury's PS.

Our analysis also shows that γ is lower during PS crossings when higher $|\mathbf{B}_{\mathrm{lobe}}|$ were observed. During active magnetic reconnection, particle scattering effects play an even more important role in the transport of particles from one magnetospheric region to another. Particles energized and accelerated by magnetic reconnection and dipolarization fronts (Sun et al., 2017, 2018) execute a larger, more chaotic gyromotion and are more likely to be lost from the flux tubes into other magnetospheric regions or shadowing of the nightside magnetopause. Furthermore, the increase of B_Z in the PS during substorm expansion phase increases the nightside loss cone angle, resulting in more particles being lost due to particle precipitation onto Mercury's nightside surface. The increased effects of particle scattering and loss cone precipitation during active reconnection contribute to enhanced loss of particles and hence, lower γ, during active time periods.

Analysis of the polytropic index γ with radial distance shows a minimum in γ at $R \sim 1.4\ R_M$. Similar feature in the radial profile of γ at Earth was reported by Frühauff et al. (2017), who suggested a connection between γ and the flow-braking region in the near-Earth magnetotail region. At Mercury, this minimum also occurs near the region where Poh et al. (2017b) reported observations of Mercury's substorm current wedge. When the reconnection rate at Mercury's dayside magnetopause (DiBraccio et al., 2013) is faster than the reconnection rate in the magnetotail, magnetic flux builds up in the two tail lobes. Substorm onset occurs during a sudden unloading of lobe magnetic flux (Slavin et al., 2010) in the highly stretched, thin PS, which launches Alfvénic Bursty Bulk Flows (BBFs), carrying dipolarized flux tubes toward Mercury. The sunward fast flows brake due to the tailward pressure gradient force as it encounters Mercury's low-β inner magnetotail region, resulting in

the diversion of plasma flow and ultimately the loss of ions from the flux tubes. The additional loss of particles due to flow braking exacerbates the problem of particle loss due to scattering and large loss cone, hence explaining the observed decrease (and minima) of γ around the flow breaking region in Mercury's magnetotail. These plasma-depleted flux tubes (or bubbles; Chen & Wolf, 1993) with low specific entropy will continue to propagate further into Mercury's inner-tail region until the increase (decrease) in plasma pressure (flux tube volume) stops its motion. This flux tube transport process is similar to that observed at Earth (e.g., Sergeev et al., 1996).

Looking into the future, the upcoming Bepi-Colombo mission, consisting of the Mercury Magnetospheric Orbiter (MMO) and Mercury Planetary Orbiter (MPO), will take our understanding of the transport of mass and energy in Mercury's magnetotail to the next level. The Mercury Ion Analyzer (MIA) and Search for Exospheric Refilling and Emitted Natural Abundances (SERENA) instrument suite will be able to obtain the full 3-D distribution function (Saito et al., 2010) and measure particle precipitation (Orsini et al., 2010), respectively, allowing us to accurately determine the plasma moments in each magnetotail regions. Advances in data sets measured by Bepi-Colombo will greatly improve our understanding of how mass and energy are transported in Mercury's magnetotail.

Acknowledgments
Data sets analyzed in this study are archived with the NASA Planetary Data System (PDS; https://pds.nasa.gov/). The authors acknowledged support provided by NASA Discovery Data Analysis Program (DDAP) grants NNX15K88G, NNX15AL01G, and NNX16AJ05G, Heliophysics Supporting Research (HSR) NNX15AJ68G, Living with a Star NNX16AJ67G, and Solar System Workings (SSW) Program grant NNX15AH28G to the University of Michigan.

References

Anderson, B. J., Acuña, M. H., Lohr, D. A., Scheifele, J., Raval, A., Korth, H., & Slavin, J. A. (2007). The Magnetometer instrument on MESSENGER. *Space Science Reviews*, *131*(1-4), 417–450. https://doi.org/10.1007/s11214-007-9246-7

Anderson, B. J., Johnson, C. L., & Korth, H. (2013). A magnetic disturbance index for Mercury's magnetic field derived from MESSENGER Magnetometer data. *Geochemistry, Geophysics, Geosystems*, *14*, 3875–3886. https://doi.org/10.1002/ggge.20242

Anderson, B. J., Johnson, C. L., Korth, H., Purucker, M. E., Winslow, R. M., Slavin, J. A., et al. (2011). The global magnetic field of Mercury from MESSENGER orbital observations. *Science*, *333*(6051), 1859–1862. https://doi.org/10.1126/science.1211001

Andrews, G. B., Zurbuchen, T. H., Mauk, B. H., Malcom, H., Fisk, L. A., Gloeckler, G., et al. (2007). The Energetic Particle and Plasma Spectrometer instrument on the MESSENGER spacecraft. *Space Science Reviews*, *131*(1-4), 523–556. https://doi.org/10.1007/s11214-007-9272-5

Angelopoulos, V., Kennel, C. F., Coroniti, F. V., Pellat, R., Kivelson, M. G., Walker, R. J., et al. (1994). Statistical characteristics of bursty bulk flow events. *Journal of Geophysical Research*, *99*(A11), 21,257–21,280. https://doi.org/10.1029/94JA01263

Baumjohann, W., & Paschmann, G. (1989). Determination of the polytropic index in the plasma sheet. *Geophysical Research Letters*, *16*(4), 295–298. https://doi.org/10.1029/GL016i004p00295

Baumjohann, W., & Treumann, R. A. (1996). *Basic space plasma physics* (p. 329). London: Imperial Coll. Press.

Borovsky, J. E., Thomsen, M. F., & Elphic, R. C. (1998). The driving of the plasma sheet by the solar wind. *Journal of Geophysical Research*, *103*(A8), 17,617–17,639. https://doi.org/10.1029/97JA02986

Büchner, J., & Zelenyi, L. M. (1989). Regular and chaotic charged particle motion in magnetotaillike field reversals: 1. Basic theory of trapped motion. *Journal of Geophysical Research*, *94*(A9), 11,821–11,842. https://doi.org/10.1029/JA094iA09p11821

Chappell, C. R., Moore, T. E., & Waite, J. H. Jr. (1987). The ionosphere as a fully adequate source of plasma for the Earth's magnetosphere. *Journal of Geophysical Research*, *92*(A6), 5896–5910. https://doi.org/10.1029/JA092iA06p05896

Chen, C. X., & Wolf, R. A. (1993). Interpretation of high-speed flows in the plasma sheet. *Journal of Geophysical Research*, *98*(A12), 21,409–21,419. https://doi.org/10.1029/93JA02080

Delcourt, D. C., Grimald, S., Leblanc, F., Berthelier, J.-J., Millilo, A., Mura, A., et al. (2003). A quantitative model of planetary Na^+ contribution to Mercury's magnetosphere. *Annales de Geophysique*, *21*(8), 1723–1736. https://doi.org/10.5194/angeo-21-1723-2003

Delcourt, D. C., Sauvaud, J.-A., Martin, R. F. Jr., & Moore, T. E. (1996). On the nonadiabatic precipitation of ions from the near-Earth plasma sheet. *Journal of Geophysical Research*, *101*(A8), 17,409–17,418. https://doi.org/10.1029/96JA01006

Deming, W. E. (1943). *Statistical adjustment of data*. New York: John Wiley.

Dewey, R. M., Slavin, J. A., Raines, J. M., Baker, D. N., & Lawrence, D. J. (2017). Energetic electron acceleration and injection during dipolarization events in Mercury's magnetotail. *Journal of Geophysical Research: Space Physics*, *122*, 12,170–12,188. https://doi.org/10.1002/2017JA024617

DiBraccio, G. A., Slavin, J. A., Boardsen, S. A., Anderson, B. J., Korth, H., Zurbuchen, T. H., et al. (2013). MESSENGER observations of magnetopause structure and dynamics at Mercury. *Journal of Geophysical Research: Space Physics*, *118*, 997–1008. https://doi.org/10.1002/jgra.50123

DiBraccio, G. A., Slavin, J. A., Imber, S. M., Gershman, D. J., Raines, J. M., Jackman, C. M., et al. (2015). MESSENGER observations of flux ropes in Mercury's magnetotail. *Planetary and Space Science*, *115*, 77–89. https://doi.org/10.1016/j.pss.2014.12.016

DiBraccio, G. A., Slavin, J. A., Raines, J. M., Gershman, D. J., Tracy, P. J., Boardsen, S. A., et al. (2015). First observations of Mercury's plasma mantle by MESSENGER. *Geophysical Research Letters*, *42*, 9666–9675. https://doi.org/10.1002/2015GL065805

Erickson, G. M., & Wolf, R. A. (1980). Is steady convection possible in the Earth's magnetotail? *Geophysical Research Letters*, *7*(11), 897–900. https://doi.org/10.1029/GL007i011p00897

Frühauff, D., Mieth, J. Z. D., & Glassmeier, K. H. (2017). Average plasma sheet polytropic index as observed by THEMIS. *Annales Geophysicae*, *35*(2), 253–262. https://doi.org/10.5194/angeo-35-253-2017

Gershman, D. J., Slavin, J. A., Raines, J. M., Zurbuchen, T. H., Anderson, B. J., Korth, H., et al. (2013). Magnetic flux pileup and plasma depletion in Mercury's subsolar magnetosheath. *Journal of Geophysical Research: Space Physics*, *118*, 7181–7199. https://doi.org/10.1002/2013JA019244

Gershman, D. J., Slavin, J. A., Raines, J. M., Zurbuchen, T. H., Anderson, B. J., Korth, H., et al. (2014). Ion kinetic properties in Mercury's pre-midnight plasma sheet. *Geophysical Research Letters*, *41*, 5740–5747. https://doi.org/10.1002/2014GL060468

Goldstein, B. E., Suess, S. T., & Walker, R. J. (1981). Mercury: Magnetospheric processes and the atmospheric supply and loss rates. *Journal of Geophysical Research*, *86*(A7), 5485–5499. https://doi.org/10.1029/JA086iA07p05485

Huang, C. Y., Goertz, C. K., Frank, L. A., & Rostoker, G. (1989). Observational determination of the adiabatic index in the quiet time plasma sheet. *Geophysical Research Letters*, *16*(6), 563–566. https://doi.org/10.1029/GL016i006p00563

Imber, S. M., & Slavin, J. A. (2017). MESSENGER observations of magnetotail loading and unloading: Implications for substorms at Mercury. *Journal of Geophysical Research: Space Physics*, *122*, 11,402–11,412. https://doi.org/10.1002/2017JA024332

Jia, X., Slavin, J. A., Gombosi, T. I., Daldorff, L. K. S., Toth, G., & van der Holst, B. (2015). Global MHD simulations of Mercury's magnetosphere with coupled planetary interior: Induction effect of the planetary conducting core on the global interaction. *Journal of Geophysical Research: Space Physics*, *120*, 4763–4775. https://doi.org/10.1002/2015JA021143

Kivelson, M. G., & Spence, H. E. (1988). On the possibility of quasi-static convection in the quiet magnetotail. *Geophysical Research Letters*, *15*(13), 1541–1544. https://doi.org/10.1029/GL015i013p01541

Korth, H., Anderson, B. J., Gershman, D. J., Raines, J. M., Slavin, J. A., Zurbuchen, T. H., et al. (2014). Plasma distribution in Mercury's magnetosphere derived from MESSENGER Magnetometer and Fast Imaging Plasma Spectrometer observations. *Journal of Geophysical Research: Space Physics*, *119*, 2917–2932. https://doi.org/10.1002/2013JA019567

Linnet, K. (1990). Estimation of the linear relationship between the measurements of two methods with proportional errors. *Statistics in Medicine*, *9*(12), 1463–1473. https://doi.org/10.1002/sim.4780091210

Orsini, S., Livi, S., Torkar, K., Barabash, S., Milillo, A., Wurz, P., et al. (2010). SERENA: A suite of four instruments (ELENA, STROFIO, PICAM and MIPA) on board BepiColombo-MPO for particle detection in the Hermean environment. *Planetary and Space Science*, *58*(1-2), 166–181. https://doi.org/10.1016/j.pss.2008.09.012

Pang, X., Cao, J. B., Liu, W. L., Ma, Y. D., Lu, H. Y., Yang, J. Y., et al. (2015). *Science China Earth Sciences*, *58*(11), 1993–2001. https://doi.org/10.1007/s11430-015-5122-6

Poh, G., Slavin, J. A., Jia, X., Raines, J. M., Imber, S. M., Sun, W.-J., et al. (2017a). Mercury's cross-tail current sheet: Structure, X-line location and stress balance. *Geophysical Research Letters*, *44*, 678–686. https://doi.org/10.1002/2016GL071612

Poh, G., Slavin, J. A., Jia, X., Raines, J. M., Imber, S. M., Sun, W.-J., et al. (2017b). Coupling between Mercury and its nightside magnetosphere: Cross-tail current sheet asymmetry and substorm current wedge formation. *Journal of Geophysical Research: Space Physics*, *122*, 8419–8433. https://doi.org/10.1002/2017JA024266

Raines, J. M., Gershman, D. J., Slavin, J. A., Zurbuchen, T. H., Korth, H., Anderson, B. J., & Solomon, S. C. (2014). Structure and dynamics of Mercury's magnetospheric cusp: MESSENGER measurements of protons and planetary ions. *Journal of Geophysical Research: Space Physics*, *119*, 6587–6602. https://doi.org/10.1002/2014JA020120

Raines, J. M., Slavin, J. A., Zurbuchen, T. H., Gloeckler, G., Anderson, B. J., Baker, D. N., et al. (2011). MESSENGER observations of the plasma environment near Mercury. *Planetary and Space Science*, *59*(15), 2004–2015. https://doi.org/10.1016/pss.2011.02.004

Rong, Z. J., Ding, Y., Slavin, J. A., Zhong, J., Poh, G., Sun, W. J., et al. (2018). The magnetic field structure of Mercury's magnetotail. *Journal of Geophysical Research: Space Physics*, *123*, 548–566. https://doi.org/10.1002/2017JA024923

Saito, Y., Sauvaud, J.-A., Hirahara, M., Barabash, S., Delcourt, D. C., Takashima, T., Asamura, K., & BepiColombo MMO/MPPE team (2010). Scientific objectives and instrumentation of Mercury Plasma Particle Experiment (MPPE) onboard MMO. *Planetary and Space Science*, *58*(1-2), 182–200. https://doi.org/10.1016/j.pss.2008.06.003

Schindler, K., & Birn, J. (1982). Self-consistent theory of time-dependent convection in the Earth's magnetotail. *Journal of Geophysical Research*, *87*(A4), 2263–2275. https://doi.org/10.1029/JA087iA04p02263

Sergeev, V. A., Angelopoulos, V., Gosling, J. T., Cattell, C. A., & Russell, C. T. (1996). Detection of localized, plasma-depleted flux tubes or bubbles in the midtail plasma sheet. *Journal of Geophysical Research*, *101*(A5), 10,817–10,826. https://doi.org/10.1029/96JA00460

Shiokawa, K., Baumjohann, W., & Haerendel, G. (1997). Braking of high-speed flows in the near-earth tail. *Geophysical Research Letters*, *24*(10), 1179–1182. https://doi.org/10.1029/97GL01062

Siscoe, G. L. (1983). Solar system magnetohydrodynamics. In R. L. Carovillano & J. M. Forbes (Eds.), *Solar-terrestrial physics, principles and theoretical foundations* (pp. 11–100). Hingham, MA: D. Reidel.

Slavin, J. A., Acuna, M. H., Anderson, B. J., Baker, D. N., Benna, M., Boardsen, S. A., et al. (2009). MESSENGER observations of magnetic reconnection in Mercury's magnetosphere. *Science*, *324*(5927), 606–610. https://doi.org/10.1126/science.1172011

Slavin, J. A., Anderson, B. J., Baker, D. N., Benna, M., Boardsen, S. A., Gloeckler, G., et al. (2010). MESSENGER observations of extreme loading and unloading of Mercury's magnetic tail. *Science*, *329*(5992), 665–668. https://doi.org/10.1126/science.1188067

Slavin, J. A., Anderson, B. J., Baker, D. N., Benna, M., Boardsen, S. A., Gold, R. E., et al. (2012). MESSENGER and Mariner 10 flyby observations of magnetotail structure and dynamics at Mercury. *Journal of Geophysical Research*, *117*, A01215. https://doi.org/10.1029/2011JA016900

Slavin, J. A., Smith, E. J., Sibeck, D. G., Baker, D. N., Zwickl, R. D., & Akasofu, S.-I. (1985). An ISEE 3 study of average and substorm conditions in the distant magnetotail. *Journal of Geophysical Research*, *90*(A11), 10,875–10,895. https://doi.org/10.1029/JA090iA11p10875

Smith, A. W., Slavin, J. A., Jackman, C. M., Fear, R. C., Poh, G.-K., DiBraccio, G. A., et al. (2017). Automated force-free flux rope identification. *Journal of Geophysical Research: Space Physics*, *122*, 780–791. https://doi.org/10.1002/2016JA022994

Spence, H. E., Kivelson, M. G., Walker, R. J., & McComas, D. J. (1989). Magnetospheric plasma pressures in the midnight meridian: Observations from 2.5 to 35 R_E. *Journal of Geophysical Research*, *94*(A5), 5264–5272. https://doi.org/10.1029/JA094iA05p05264

Sun, W. J., Fu, S. Y., Slavin, J. A., Raines, J. M., Zong, Q. G., Poh, G. K., & Zurbuchen, T. H. (2016). Spatial distribution of Mercury's flux ropes and reconnection fronts: MESSENGER observations. *Journal of Geophysical Research: Space Physics*, *121*, 7590–7607. https://doi.org/10.1002/2016JA022787

Sun, W. J., Raines, J. M., Fu, S. Y., Slavin, J. A., Wei, Y., Poh, G. K., et al. (2017). MESSENGER observations of the energization and heating of protons in the near-Mercury magnetotail. *Geophysical Research Letters*, *44*, 8149–8158. https://doi.org/10.1002/2017GL074276

Sun, W. J., Slavin, J. A., Dewey, R. M., Raines, J. M., Fu, S. Y., Wei, Y., et al. (2018). A comparative study of the proton properties of magnetospheric substorms at Earth and Mercury in the near magnetotail. *Geophysical Research Letters*, *45*, 7933–7941. https://doi.org/10.1029/2018GL079181

Sun, W.-J., Slavin, J. A., Fu, S., Raines, J. M., Zong, Q.-G., Imber, S. M., et al. (2015). MESSENGER observations of magnetospheric substorm activity in Mercury's near magnetotail. *Geophysical Research Letters*, *42*, 3692–3699. https://doi.org/10.1002/2015GL064052

Sundberg, T., Slavin, J. A., Boardsen, S. A., Anderson, B. J., Korth, H., Ho, G. C., et al. (2012). MESSENGER observations of dipolarization events in Mercury's magnetotail. *Journal of Geophysical Research*, *117*, A00M03. https://doi.org/10.1029/2012JA017756

Zelenyi, L., Oka, M., Malova, H., Fujimoto, M., Delcourt, D., & Baumjohann, W. (2007). Particle acceleration in Mercury's magnetosphere. *Space Science Reviews*, *132*(2-4), 593–609. https://doi.org/10.1007/s11214-007-9169-3

Zhong, J., Wei, Y., Pu, Z. Y., Wang, X. G., Wan, W. X., Slavin, J. A., et al. (2018). MESSENGER observations of rapid and impulsive magnetic reconnection in Mercury's magnetotail. *The Astrophysical Journal*, *860*(2), L20. https://doi.org/10.3847/2041-8213/aaca92

Zhu, X. M. (1990). Plasma sheet polytropic index as inferred from the FPE measurements. *Geophysical Research Letters*, *17*(13), 2321–2324. https://doi.org/10.1029/GL017i013p02321